Finite-difference time-domain modeling and experimental characterization of planar waveguide fluorescence sensors

Jyrki S. Kimmel and Douglas A. Christensen*

Department of Bioengineering, and *Department of Electrical Engineering
University of Utah, Salt Lake City, UT 84112

ABSTRACT

The finite-difference time-domain method (FDTD) is a powerful numerical technique for solving Maxwell's equations in a discretized space and time grid. Its applications have up to now been in the analysis of electrically large structures in the microwave domain, and the scope of investigations has been extended to the optical region only recently. Because of computer memory limitations, the method is generally restricted to configurations which extend to the order of tens of wavelengths in three dimensions, or hundreds of wavelengths in two dimensions. Optical sensor structures are therefore of suitable size to be modeled with FDTD, and *e. g.* fluorescence sensor design can benefit from the use of FDTD in optimization of the waveguide structures. In general, the integration of chemical and optical design is difficult, but FDTD can bring the two design approaches closer together. One of the main advantages of FDTD is its ability to include near-field effects, such as distribution of protein molecules on the active surface of optical sensors in the model, which has been shown to be important in estimating the fluorescent excitation and collection efficiencies of molecules on surfaces. In addition, for planar structures, two-dimensional models are adequate for studying many aspects of sensor design. We applied FDTD to design of planar fluorescence sensors. Excitation and emission models were analyzed for planar waveguide structures with side collection of emitted light in mind. Planar waveguides were fabricated on fused silica substrates, and the characteristics of the waveguides were compared to the model. Good agreement was found with the FDTD modeling to the physical model, and based on this knowledge, an FDTD sensor model was prepared predicting good fluorescence excitation and emission side collection efficiencies.

1. INTRODUCTION

Yee first introduced FDTD as a numerical method for solving Maxwell's equations in 1966[1], and the pioneering works on the application of this technique in the microwave domain were done by Taflove[2]. Recently, the scope of FDTD has been extended to the optical range of frequencies, as suitable problems to be analyzed with the method have emerged[3]. Planar optical sensors are particularly good candidates to be modeled with FDTD. Their structure is simple enough for the

0-8194-0718-6/92/$4.00

model to be used effectively, and due to the planarity, only a two-dimensional analysis is required for many cases. With a modern-day supercomputer, structures of hundreds of wavelengths long can be analyzed in two dimensions.

FDTD is an initial-value problem, where an electromagnetic field evolves, as specified by the sources, in discrete time steps along a lattice including the structure to be analyzed. The propagation of the field is affected by the complex dielectric constants at each lattice point (cell), and at boundaries with differing complex permittivities, reflection, refraction and diffraction can be observed. The time-stepping is carried out to several complete cycles of a sinusoidally varying source, until the source fields have propagated through the whole model space, and maximum values of the field component magnitudes during a half-cycle after the last complete cycle are stored. Thus, a steady-state solution of the field components is achieved for each cell in the model space.

In the analysis, great care must be taken in choosing the boundary conditions. Since FDTD is an initial-value time-domain method, the propagating wave will reflect at the outer lattice boundaries unless special conditions are imposed on the fields at the boundary cells to make them absorbing while minimizing reflections at the absorber interface. We have used the double precaution of lining the entire area of the lattice with a four-cell layer of an absorber in addition to employing Mur second-order absorbing boundary conditions[4]. This prevents a significant amount of energy from reflecting at the lattice boundaries. Although the absorbing boundaries extend the limits of the lattice and thus reduce space of the structure to be analyzed, FDTD presents savings in memory and execution time. Whereas other methods require storage and computation time on the order of $(3N)^2$ and $(3N)^3$, respectively, where N is the number of cells in the model, FDTD requires only N for both. This is a direct consequence of the time-domain aspect of the method.

The structure analyzed with FDTD can include features down to one cell in size, which is an important advantage in the analysis of near-field effects. Since the lattice is usually made of cells in the order of a tenth of a wavelength, features of a few tens of nanometers can be included in models in the optical region. These features can be sources, or absorbers and scatterers.

We fabricated doped quartz-on-silica waveguides designed according to a previously published FDTD modeling study[5], and then compared the waveguides to an FDTD model. The measured physical characteristics of the waveguides were then applied to an FDTD model to predict the performance of the components in fluorescence sensing.

2. THEORY

The starting point for the FDTD analysis is the general Yee lattice unit cell as shown in Fig. 1. Maxwell's equations in a rectangular coordinate system, which are

$$-\partial B_x / \partial t = \partial E_z / \partial y - \partial E_y / \partial z \quad (1a)$$

$$-\partial B_y / \partial t = \partial E_x / \partial z - \partial E_z / \partial x \quad (1b)$$

$$\partial B_z / \partial t = \partial E_x / \partial y - \partial E_y / \partial x \quad (1c)$$

$$\partial D_x / \partial t = \partial H_z / \partial y - \partial H_y / \partial z - J_x \quad (1d)$$

$$\partial D_y / \partial t = \partial H_x / \partial z - \partial H_z / \partial x - J_y \quad (1e)$$

$$\partial D_z / \partial t = \partial H_y / \partial x - \partial H_x / \partial y - J_z \quad (1f)$$

can be discretized in a lattice formed of such cells by finite-difference equations as follows[1]:

$$[B_x^{n+1/2}(i, j + 1/2, k + 1/2) - B_x^{n-1/2}(i, j + 1/2, k + 1/2)] / \Delta t$$

$$= [E_y^n(i, j + 1/2, k + 1) - E_y^n(i, j + 1/2, k)] / \Delta z - [E_z^n(i, j + 1, k + 1/2) - E_z^n(i, j, k + 1/2)] / \Delta y \quad (2)$$

for (1a), and

$$[D_x^n(i + 1/2, j, k) - D_x^{n-1}(i + 1/2, j, k)] / \Delta t$$

$$= [H_z^{n-1/2}(i + 1/2, j + 1/2, k) - H_z^{n-1/2}(i + 1/2, j - 1/2, k)] / \Delta y$$

$$- [H_y^{n-1/2}(i + 1/2, j, k + 1/2) - H_y^{n-1/2}(i + 1/2, j, k - 1/2)] / \Delta z + J_x^{n-1/2}(i + 1/2, j, k) \quad (3)$$

for (1d), where (i,j,k) are the spatial indices for the cell, and the superscript n represents the n^{th} time value of the field. Discretization for the other equations (1b-c, e-f) can be obtained similarly to (2-3). A two-dimensional model based on the Yee lattice discretization was used in this study.

3. FABRICATION AND CHARACTERIZATION OF PLANAR WAVEGUIDE COMPONENTS

3.1. Waveguide fabrication

Waveguides were fabricated for the purposes of this study by principles shown in a previous theoretical study[5]. Fused silica substrates (grade S1-UV) were obtained from Esco Products Inc., precleaned with acetone, methanol and deionized

water, dried with nitrogen gas, and placed in the sputtering chamber of a MRC 822 sputtersphere together with a <111> n-type silicon wafer. A SiO_2 sputtering target was used with Ar and N_2 in the chamber for doping the quartz to attain a higher refractive index than what is possible with plain argon sputtering. The samples were sputtered for 270 minutes with an average RF power of 380 W in a base pressure of $6 \cdot 10^{-6}$ torr, and with argon pressure of 7.8 μmHg, and N_2 pressure of 1.2 μmHg.

3.2. Waveguide characterization

The waveguides were characterized by measuring the mode angle and loss (see Fig. 2). Also the thickness and refractive index were measured by ellipsometry on the silicon wafer sample. The internal mode angle measurement was done by prism-coupling TM-polarized green HeNe laser light at 534.5 nm through a SF-6 prism (Karl Lambrecht Co.) into the waveguiding layer, and then measuring the light power coming out of the waveguide with different internal coupling angles. The maximum outgoing power was obtained at an internal prism coupling angle of 53.52 degrees, as can be seen from Fig. 3. The corresponding mode angle in the waveguide was found to be 85.04 degrees, with waveguide thickness 1.38 μm and refractive index 1.4672 as calculated with programs provided by Jeff Ives[6]. The ellipsometry study was performed with a Rudolph Research ellipsometer at 65.2 and 67.55 degree incidence angles. The results are in fairly good agreement with the ones obtained from mode angle measurement, giving waveguide refractive index of 1.464 at 632.8 nm, and thickness of 1.42 μm. At 543.5 nm the refractive index would be 1.467, assuming identical dispersion to the substrate material (see section 4.1).

The loss was measured by prism-coupling 534.5 nm light into the waveguide and imaging the waveguide with a CCD camera (Photometrics Series 200), as described in detail elsewhere[7]. The intensity in the image of the streak of light gave the attenuation as a function of distance traveled by the light in the waveguide. Taking the logarithm of the intensity *vs.* the distance gives a rather high loss of 6 dB/cm (see Fig. 4).

4. FDTD MODELS OF A PLANAR WAVEGUIDE FLUORESCENCE SENSOR

We have reported previously on optimization results for planar fluorescence sensor structures[5]. The strategy in the study was to develop a model for a single-mode waveguide which would be weakly guiding for TM-polarized excitation light, while being cutoff for emission at a longer wavelength. Therefore, no light from fluorescent emission would be guided in the waveguide, and more emission could be collected passing through the substrate of the waveguide. The results of the study gave guidelines for the design of these components, which were fabricated as explained in section 3.1. The waveguides were then characterized experimentally, and physically realistic two-dimensional FDTD models were subsequently developed based on the measurements (see section 3.2.). First, to compare the measured characteristics of the components, a model with identical physical characteristics to the waveguide was made. This model had no sensor function, as air was used as a superstrate. Then, sensor-related models were developed separately both for excitation and emission of fluorescence.

4.1 Model to compare FDTD to characterization studies of the waveguides

The model used in both comparing FDTD to the physical characterization of the waveguides and sensor modeling is shown in Fig. 5. For the first case, the superstrate was air (refractive index n=1.00 + i·0.00). The refractive index of the quartz substrate at 543.5 nm was estimated by a third-order polynomial interpolation from the supplier's data sheet[8] to be 1.4601 + i·0.00. The observed waveguide refractive index was 1.4672+ i·0.00. Based on these values, the boundary conditions were determined for minimum reflectance at 45 degree incidence angle, for the superstrate region and substrate region separately. The analysis gave absorber conductivities of $2.5457 \cdot 10^4\ \Omega^{-1}m^{-1}$ and $5.4270 \cdot 10^4\ \Omega^{-1}m^{-1}$, respectively. The 1.38 μm waveguide thickness was modeled with 30 unit cells, each 46 nm in size, and the total dimensions of the model were 9.2 μm by 18.4 μm for the 200 by 400 unit cell model space. The excitation source was assumed to be a 12 element line source array oscillating sinusoidally at $5.51978 \cdot 10^{14}$ Hz (for free space wavelength of 543.5 nm). The magnitudes of the E_x fields at the source segments were weighted according to the field distribution shown in Fig. 6, as determined from the Ives model[6].

4.2 Excitation and emission sensor models

The physical dimensions and cell spacing of the excitation and emission models were kept as designed in the previous section, and to correspond to the fabricated sensor, fused silica substrates, with nitrous quartz waveguides formed on the sensing surface were assumed. We also included an immobilized 92 nm thick protein layer on the waveguide-superstrate interface. The superstrate was assumed to be water, for which the refractive index was determined to be 1.3346 + i·0.00 at 543.5 nm by third-order polynomial interpolation of data from the AIP Handbook[9]. The refractive index of protein was assumed to be 1.497 + i·0.00. These values were used for excitation modeling. The absorber conductivity for the region adjacent to the superstrate was now changed to $4.5340 \cdot 10^4\ \Omega^{-1}m^{-1}$. The same excitation source as in the previous section was used for this model as well.

To analyze the behavior of the emission, the waveguide properties were interpolated to 570 nm giving n = 1.4590 + i·0.00 for the substrate, and n = 1.3336 + i·0.00 for the water superstrate. The waveguide refractive index difference Δn = 0.0071 was maintained, and the refractive index of the protein was also assumed to change by the same percentage as the index of the substrate, giving n = 1.4959. The absorbing boundary conditions were designed for this wavelength again, and the conductivities were assigned at $4.3171 \cdot 10^4\ \Omega^{-1}m^{-1}$ and $5.1669 \cdot 10^4\ \Omega^{-1}m^{-1}$ for the superstrate and substrate, respectively. Fluorescent emission with frequency $5.26316 \cdot 10^{14}$ Hz (which corresponds to a 570 nm free space wavelength) was modeled by creating five 25 cell wide random source distributions in the protein layer adjacent to the waveguide. Each cell in the source distribution had an even chance of being a source, and in turn had an even chance of being oriented in the x or y direction. In addition, each source had a uniformly distributed random phase. An example of a source layer is shown in Fig. 7.

4.3. Computer resources and program features

The models were analyzed by an FDTD program written in Fortran-77 in the University of Utah Department of Electrical Engineering. The program was run on an HP-9000 Unix-based computer. For the 200 by 400 cell model, the program required approximately one hour of CPU time using 50 source oscillation cycles.

The program provides integration of the normal component of the Poynting vector at a half-closed rectangular surface extending from the location of the sources to the end of the model space, with an arbitrary z-dimension. This integral multiplied by two gives the total power generated by the sources, assuming symmetry about the sources. The value of the normal component of the Poynting vector can also be integrated across the waveguide and the adjacent protein layer. These values are used to determine the efficiency of excitation and the power carried by the waveguide for the emission and excitation by calculating the ratio of integrated Poynting vector in the waveguide or protein layer and the total integrated Poynting vector in the half-space containing the end of the waveguide.

Another important feature of the program is that it averages the dielectric constant of adjacent cells. This is useful because otherwise, as the magnetic field component is always calculated a half cell distance away from where the electric field is determined, at surfaces with different dielectric constants in adjacent cells, the magnetic field component of a cell may in fact be calculated with an incorrect value of the dielectric constant, which will result in minor errors in analyses.

5. RESULTS AND DISCUSSION

The sensor components fabricated with the sputtering method were found to be single-mode near-cutoff structures. The losses of 6 dB/cm are nearly unacceptable for a direct fluorescence sensor. Scattering seemed to be the dominant loss mechanism, which for energy-transfer based sensing schemes may not be an important factor.

The results of the comparison of FDTD model to the measured characteristics of the components at the end of the model space ($y = 388$) are shown in Fig. 8. The FDTD model gives a slightly wider electric field distribution in the x-direction (E_x component) than the physical model, which may be a result of inaccuracies in the measurements. In addition, some kinks are observed near the maximum field values indicating possible back-reflections from the end face of the model space. The ripples at the substrate side of the model are probably due to evolving substrate modes due to the truncation of the model space at 200 cells. At the waveguide-superstrate interface, which is the region of interest, the FDTD model performs very well.

The results from sensor modeling are shown in Fig. 9. For excitation modeling, the Ives model[6] agrees as well with the FDTD model as in the previous case, and similar characteristics are seen in the excitation FDTD model. The Poynting

vector integration shows that 60 % of light energy is propagating in the waveguide, and 3.1 % in the protein layer at y = 388. This means that fluorescence excitation is possible with this sensor configuration.

As for the emission modeling, Fig. 9 shows that the averaged source distributions give a highly radiative E_x component across the component. Indeed, only 0.88 % of light energy is found to propagate in the waveguide at y =388, which means the original rationale for maximizing side-collection efficiency is supported by this study.

In summary, FDTD modeling is shown to produce realistic results in fluorescence sensor design. Further work is needed in the area of assigning optical properties to the protein layers in order to bring the chemical design closer to optical modeling and to predict sensor responses more accurately.

6. ACKNOWLEDGEMENTS

The authors wish to thank the personnel of the HEDCO microelectronics laboratory of the University of Utah for valuable help in fabricating the waveguides, Mr. Jinyu Wang for assistance in the ellipsometer measurements, and Ms. Shellee Dyer for her help in waveguide loss measurements. J. S. K. wishes to express his gratitude to the following organizations who have contributed to this research by scholarships, funds and grants: Technical Research Centre of Finland, Academy of Finland, Instrumentarium Science Foundation, Finland-U.S. Educational Exchange Commission, Tampere University of Technology, and United States Information Service.

7. REFERENCES

1. K. S. Yee, "Numerical solution of initial boundary value problems involving Maxwell's equations in isotropic media," *IEEE Transactions on Antennas and Propagation*, vol. AP-14, pp. 302-307, May, 1966.

2. A. Taflove, "Application of the finite-difference time-domain method to sinusoidal steady-state electromagnetic-penetration problems," *IEEE Transactions of Electromagnetic Compatibility*, vol. EMC-22, pp. 191-202, August, 1980.

3. D. A. Christensen and J. Andrade, "Analysis of efficiency of fluorescent coupling in guided-wave immunosensors", presented at *Biosensors '90*, Singapore, May 2-4, 1990.

4. G. Mur, "Absorbing boundary conditions for the finite-difference approximation of the time-domain electromagnetic field equations", *IEEE Transactions of Electromagnetic Compatibility*, vol. EMC-23, pp. 377-382, 1981.

5. J. S. Kimmel and D. A. Christensen, "FDTD Modeling in the design of optical chemical sensor structures", presented at *Transducers '91, The 6th International Conference on Solid-State Sensors and Actuators*, San Francisco, June 23-27, 1991.

6. J. Ives, Optical waveguide sensors: Characterization of evanescent and scatter excitation. PhD dissertation, University of Utah, 1990.

7. J. S. Kimmel, S. Dyer, and D. A. Christensen, "Waveguide Loss Measurement by CCD Imaging", to be published, 1991.

8. ESCO Product Catalog, ESCO Products, Inc. Oak Ridge, NJ, 1987.

9. D. E. Gray (editor), American Institute of Physics Handbook, Third Edition, p. 6-105, McGraw Hill Book Company, New York, 1972.

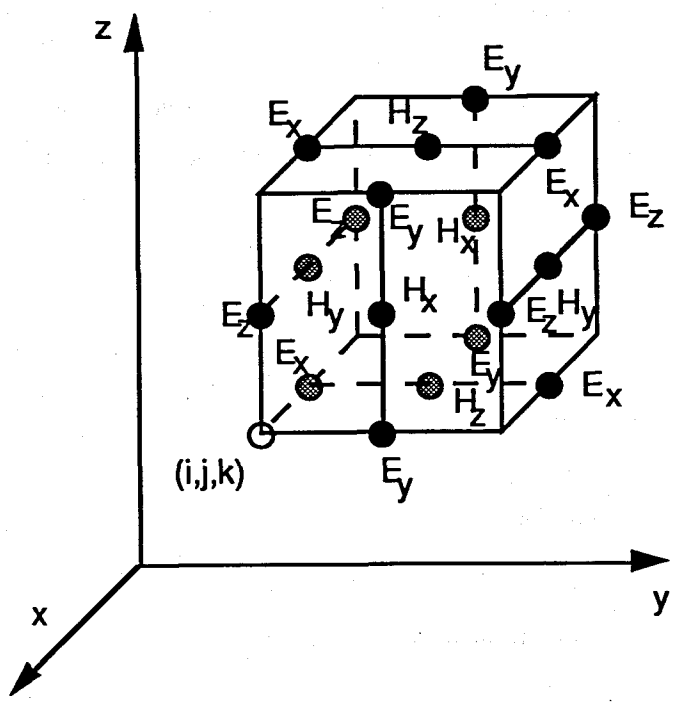

Fig. 1. Unit cell in a three-dimensional Yee lattice[1].

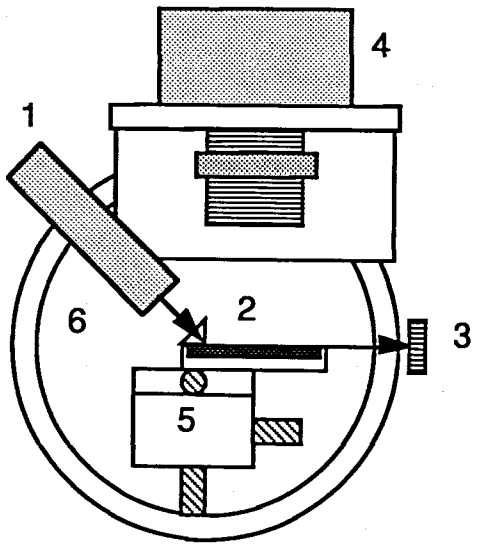

Fig. 2. Experimental arrangement. 1: Green HeNe laser (543.5 nm), 2: Waveguide holder with coupling prism, 3: Power meter, 4: CCD camera, 5: XYZ stage, 6: Goniometer base.

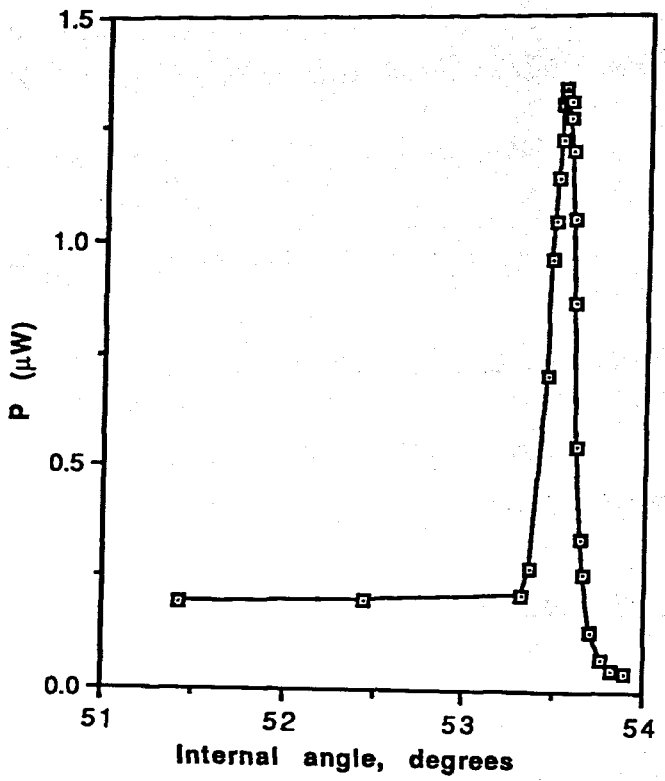

Fig. 3. Waveguide coupling angle measurement: outgoing power *vs.* coupling angle at 0.57 mW input power.

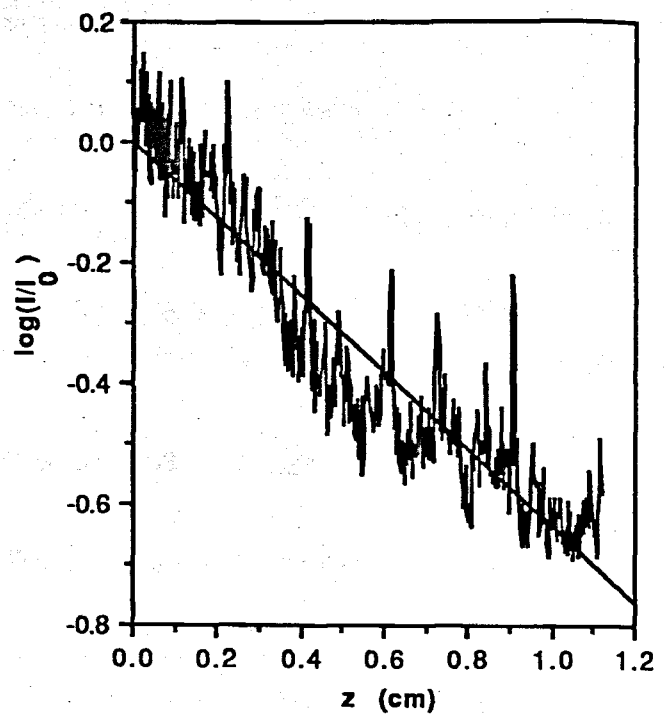

Fig. 4. Waveguide loss measurement. The straight line is a least-squares fit to the CCD data giving a loss of 6 dB/cm.

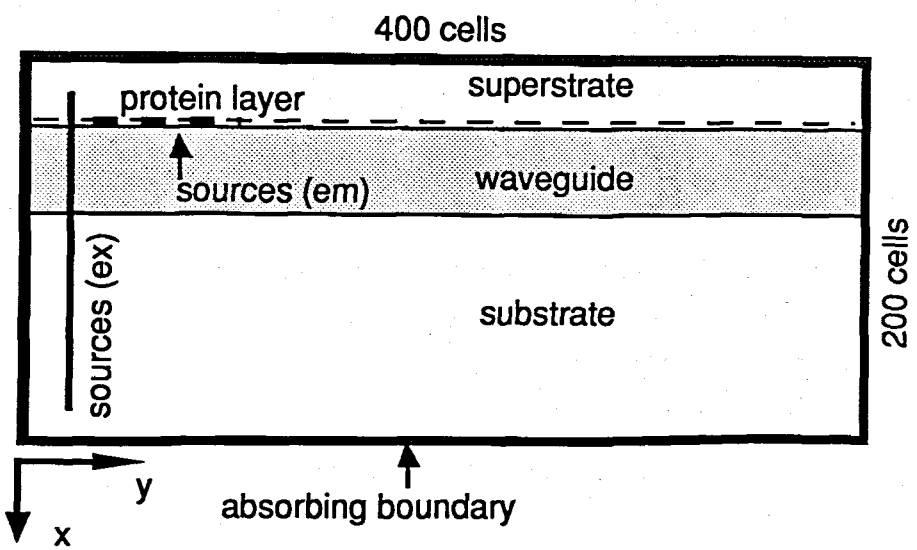

Fig. 5. FDTD model space. The entire 200 by 400 cell (9.2 μm by 18.4 μm) model is lined inside with a 4 cell wide absorber. The source locations are shown for excitation (ex) and emission (em) models. The figure is not to scale.

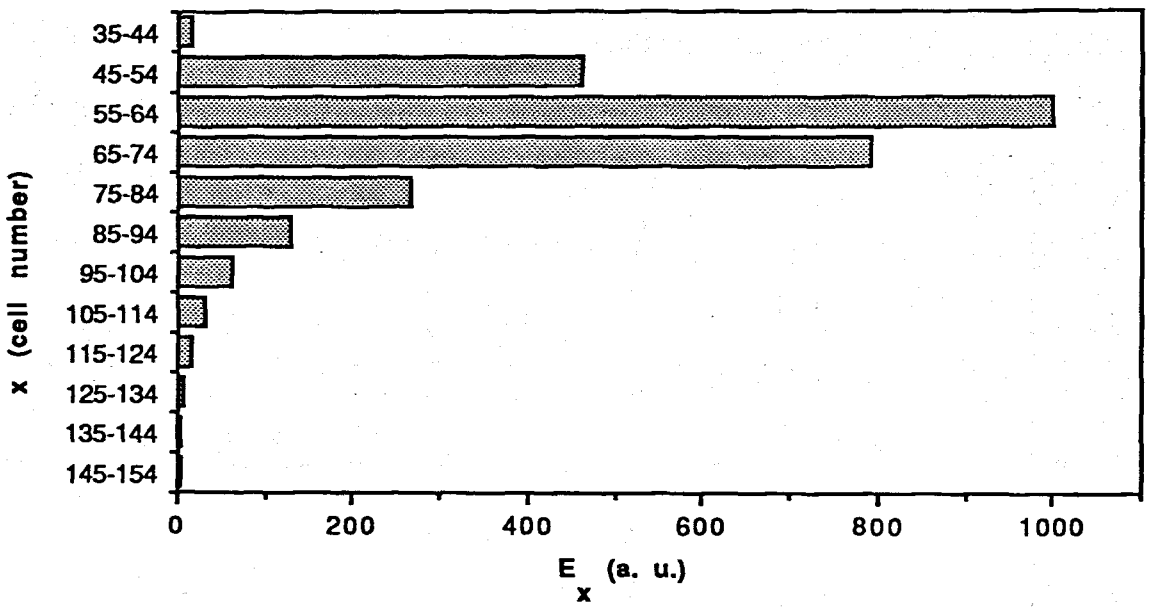

Fig. 6. Excitation model source distribution.

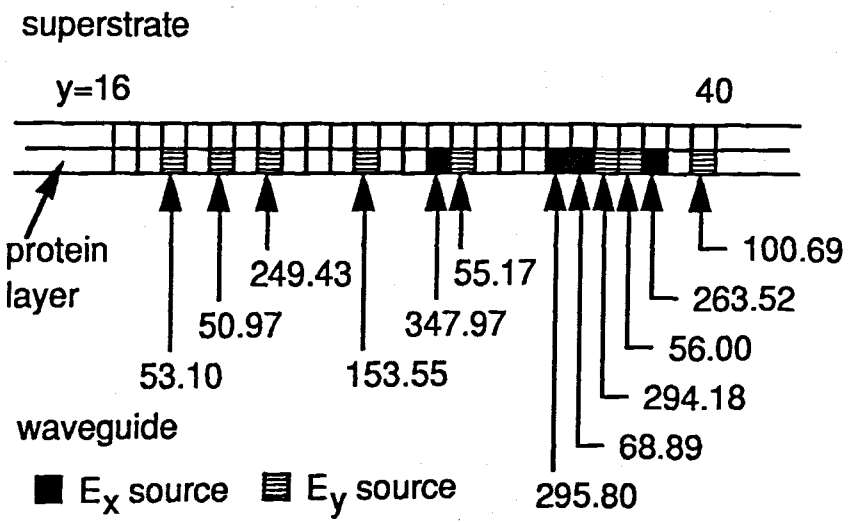

Fig. 7. Example of emission model source distribution. The numbers designate the phases of the individual source elements, in degrees.

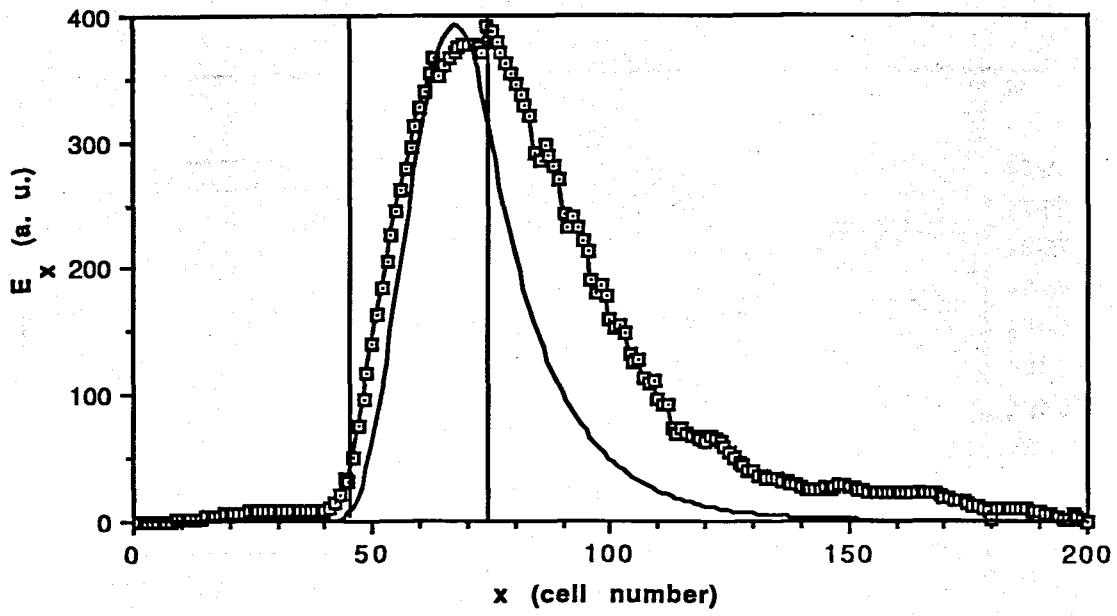

Fig. 8. Comparison of the characterization results (solid curve) of the waveguide to FDTD modeling (open squares) at y = 388. The vertical lines represent the borders of the waveguide with superstrate on the far left and substrate on the far right.

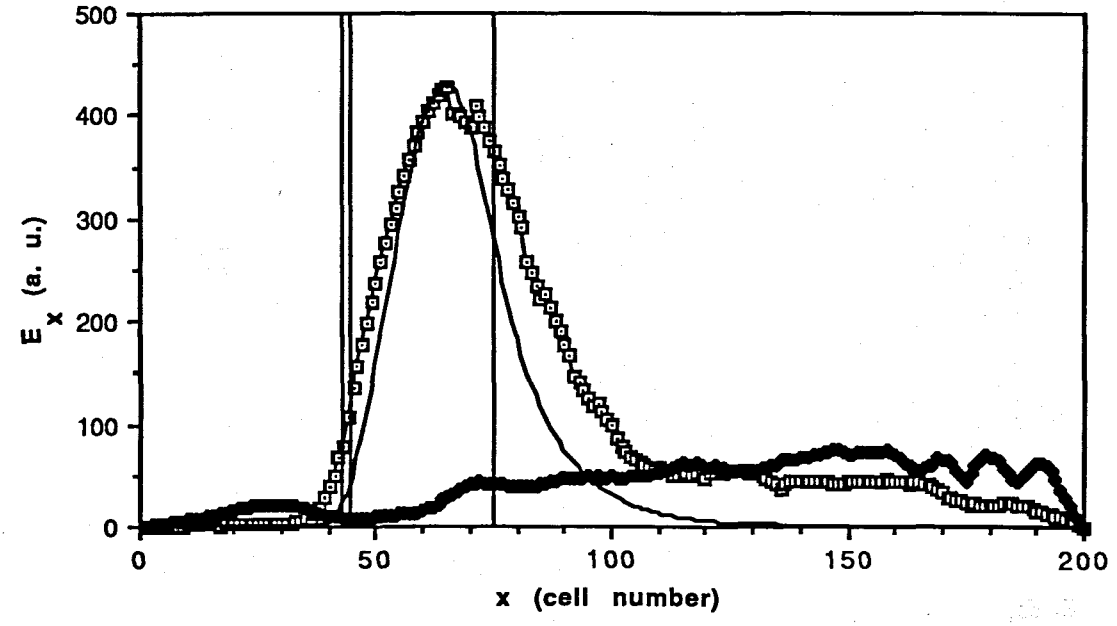

Fig. 9. Results of FDTD sensor modeling at y = 388. Solid curve: Ives model[6], open squares: excitation model, closed diamonds: averaged emission model. The double vertical line represents the location of protein layer on the waveguide at the superstrate interface, and the single vertical line shows the waveguide-substrate interface.